Universiteit
Leiden
The Netherlands

Growing oxide thin films in a low-energy electron microscope

Torren, A.J.H. van der

Citation
Torren, A. J. H. van der. (2016, December 5). *Growing oxide thin films in a low-energy electron microscope*. *Casimir PhD Series*. Retrieved from https://hdl.handle.net/1887/44732

Version:	Not Applicable (or Unknown)
License:	Licence agreement concerning inclusion of doctoral thesis in the Institutional Repository of the University of Leiden
Downloaded from:	https://hdl.handle.net/1887/44732

Note: To cite this publication please use the final published version (if applicable).

Cover Page

Universiteit Leiden

The handle http://hdl.handle.net/1887/44732 holds various files of this Leiden University dissertation

Author: Torren, Alexander J.H. van der
Title: Growing oxide thin films in a low-energy electron microscope
Issue Date: 2016-12-05

6

Finding signatures of the conducting $LaAlO_3/SrTiO_3$ interface at the growth temperature by electron reflection

The two-dimensional electron gas occurring between the band insulators $SrTiO_3$ and $LaAlO_3$ has attracted a lot of interest. The formation of this conducting interface is sensitive to the growth conditions, but despite numerous investigations, there are still questions about the details of the physics involved. In particular, not much is known about the electronic structure of the growing $LaAlO_3$ layer at the growth temperature (around 800°C) in oxygen (pressure around 5×10^{-5} mbar), since analysis techniques at these conditions are not readily available. For this we developed a pulsed laser deposition system inside our low-energy electron microscope. Our setup allows for layer-by-layer growth control and in-situ measurements of the angle-dependent electron reflection intensity. This gives information on the surface layers as a fingerprint of their electronic structure during the growth.

This chapter will be submitted as:

A.J.H. van der Torren, Z. Liao, C. Xu, N. Gauquelin, C. Yin, J. Aarts, S.J. van der Molen,
Finding signatures of the conducting $LaAlO_3/SrTiO_3$ interface at the growth temperature by electron reflection

6.1 Introduction

Transition metal oxides, and in particular perovskites, form an exciting class of materials exhibiting a variety of physical phenomena such as superconductivity, magnetism and ferroelectricity. Expecially interesting for possible electronics applications was the discovery of the formation of a two-dimensional electron gas between the two band insulators $LaAlO_3$ and $SrTiO_3$ [1]. The emergence of this conducting interface can at least partially be explained by the so-called polar catastrophe model. In this model an increasing electrical potential builds up when charged $(LaO)^+$ and $(AlO_2)^-$ layers are alternatively stacked on top of neutral $SrTiO_3$. This potential is compensated by the transfer of half an electron from the surface to the interface. A relevant observation is that the electron gas only forms when the top $LaAlO_3$ layer is at least four unit cells thick [2]. Only for this thickness the potential buildup is apparently enough to transfer the electron to the interface. Furthermore, the electron gas only forms at the n-type interface (TiO_2/AlO_2) and not at the p-type interface (SrO/LaO) [1]. At the p-type interface a structural reconstruction is energetically favorable above the electronic reconstruction [3].

While these observations are in favor of the electronic reconstruction, defects in the crystal and in particular in the TiO_2-layer, also play an important role in the formation of the electron gas. Not surprisingly, therefore, it is very much the growth conditions which determine the conducting properties of the interface. Pulsed laser deposition (PLD) is the most commonly used technique to grow $LaAlO_3/SrTiO_3$ heterostructures. Here the exact plume shape and composition as well as the oxygen pressure are of great importance, influencing the cationic stoichiometry [4–6] of the $LaAlO_3$ film and the number of oxygen vacancies in the $SrTiO_3$ [7]. A La/Al-ratio exceeding 0.97 [4] has been shown to totally suppress the conductivity. Furthermore, magnetism [7–10] and superconductivity [11–13] have been shown to occur at low temperatures, depending on the oxygen pressure during growth.

Whereas differences in growth conditions are known to lead to conducting or insulating samples as measured afterwards, little is known about how the electronic properties of the material develop during growth. Unfortunately, electrical measurements are very difficult at the high growth temperatures.

Also, the high temperatures and high oxygen pressure required during growth limit the abilities for in-situ analysis. Most techniques cannot work in this environment. For this reason we recently developed an in-situ pulsed laser deposition system for our low-energy electron microscope. This not only allows for layer-by-layer growth control and structural information but also allows measurements of the electron reflectivity of the surface with sub-unit cell precision, which yields information on the empty band structure [14].

Here we use this information to investigate the differences in (surface) electronic structure between conducting and insulating samples. We will focus on the changing electron reflectivity during growth at the growth temperature.

6.2 Experimental setup and sample preparation

The $LaAlO_3/SrTiO_3$ interfaces are grown and studied in an aberration corrected low-energy electron microscope (LEEM) at Leiden university, called ESCHER [15–18]. This technique has been used before to study $SrTiO_3$ [19] and $LaAlO_3$ [20] separately but now a pulsed laser deposition (PLD) system has been developed inside the LEEM to allow for analysis during growth, see chapter 5. In order to study growth, pulsed deposition is performed alternatingly with LEEM imaging. In more detail, between every few pulses deposited, the LEEM is turned on (i.e. the high voltage between objective lens and sample, required for the low-energy electrons, is turned on) and diffraction images are obtained. From the diffraction images the intensity and shape of the specular diffraction spot is investigated for layer-by-layer growth control. After this measurement the high voltage is turned off and deposition can continue. For the layer-by-layer growth control we obtain the full-width-half-max (FWHM) and peak intensity of the specular spot. The FWHM and intensity oscillate with the surface roughness due to spot broadening. To obtain a fingerprint of the unoccupied band structure, angle-resolved reflected electron spectroscopy (ARRES) is also performed [14]. In this technique the electron reflection is measured depending on energy and in-plane wave vector. For the ARRES measurements we obtain the total spot intensity which is independent of the surface roughness i.e. the total intensity stays constant when the surface roughens since the spot broadening lowers the maximum.

As substrates, $SrTiO_3$ (100) single crystals from CrysTec GmbH are used which are TiO_2-terminated by a buffered HF etch [21] and annealing in oxygen at 950 °C for one hour. The SrO-terminated substrate was prepared in a different PLD system by growing a double SrO-layer on a TiO_2-terminated substrate. For the PLD targets, single crystals $LaAlO_3$ (100) from Crystal GmbH were used. The PLD growth is performed at a pressure of 5.5×10^{-5} mbar oxygen and if not otherwise stated at a 2 J/cm^2 laser fluence with 1 Hz repetition rate. Depending on deposition speed, the deposition is briefly intermitted each 5 to 50 pulses to perform imaging and spectroscopy. This results in around 10 measurements per unit cell grown. Samples are grown at temperatures between 800 and 860 °C as measured with a pyrometer (emissivity 0.8). Temperature-dependent resistance measurements were performed in a Physical Properties Measurement System (PPMS, Quantum Design) in a van der Pauw configuration. In order to facilitate the discussion, samples with a conducting interface will henceforth be designated with the suffix "C", insulating samples will be labeled "I".

6.3 Results

Three $LaAlO_3/SrTiO_3$ heterostructures were grown under two different growth conditions and on two kind of substrates. The first sample (S1-C) was grown with an optimal fluence of 2 J/cm^2 on a TiO_2-terminated $SrTiO_3$-substrate, the second sample (S2-I) was grown with a much lower fluence by defocusing the PLD laser on the same TiO_2-terminated substrate, and the third sample (S3-I) was grown with

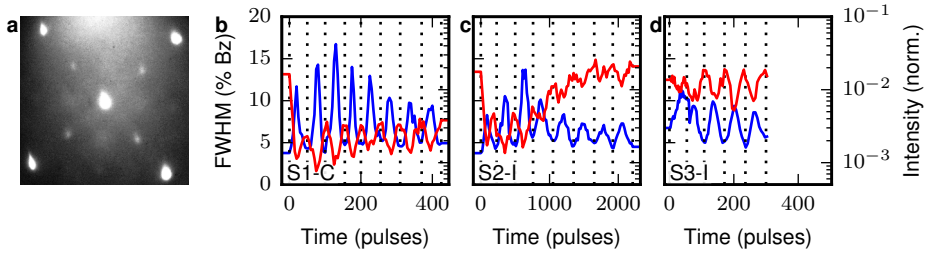

FIGURE 6.1: a) Diffraction pattern on bare $SrTiO_3$ at a growth temperature of 820 °C taken at 17 eV. b) FWHM (blue) and maximum intensity (red) of the specular diffraction spot for a conducting sample S1-C. c) Same for the insulating sample S2-I and d) same for the insulating sample S3-I. All data have been taken at 17 eV landing energy. The FWHM is given in percentage of the Brillouin zone, which is equal to the percentage of the distance from specular to the first order spots. The intensity has been normalized at the mirror mode (zero landing energy) intensity.

the optimal fluence of 2 J/cm^2 on the SrO-terminated $SrTiO_3$-substrate. For layer-by-layer growth control we took low-energy electron diffraction images as shown in fig. 6.1a for bare $SrTiO_3$. From the diffraction images, the peak intensity and full-width-half-maximum (FWHM) of the specular spot were recorded and are shown in fig. 6.1b, c, d in red and blue respectively for samples S1-C, S2-I and S3-I.

Clear oscillations can be observed in both FWHM and peak intensity, which are out of phase with one another. The landing energy of the electrons (17 eV) has been optimized for maximal contrast in the oscillations. This energy is close to the out-of-phase conditions where the electrons destructively interfere at the step edges on the surface. The oscillations can be understood by comparing a flat and rough surface. At the flat surface, typical for a fully grown unit cell layer, the electron constructively interfere along the out-of-plane axis of the crystal, resulting in a sharp diffraction spot (i.e. high peak intensity and small FWHM). On the other hand, at the rough surface (i.e. at n + 1/2 unit cell grown) the electrons interfere destructively at the new grown islands and scatter around, resulting in a broad diffraction peak (i.e. low peak intensity and high FWHM). As a guide to the eye, dotted lines are plotted to indicate integer number of unit cells grown. A total of eight unit cells was grown on S1-C, S2-I and five unit cells on S3-I. Much more pulses were needed for sample S2-I (Fig. 6.1c) than sample S1-C and S3-I (Fig. 6.1b, d). From this we can conclude that the growth speed is highly reduced for the out-of-focus laser beam, as expected.

For sample S1-C (Fig. 6.1b) the peak intensity strongly decreases at the start to oscillate around a constant background for the remainder of the time. Sample S2-I shows the same decrease but the background increases back to the starting value between three and five unit cells. Finally sample S3-I does not show the decrease at the start and keeps oscillating around a constant value. This change in background intensity is related to the electronic structure of the surface layer as we

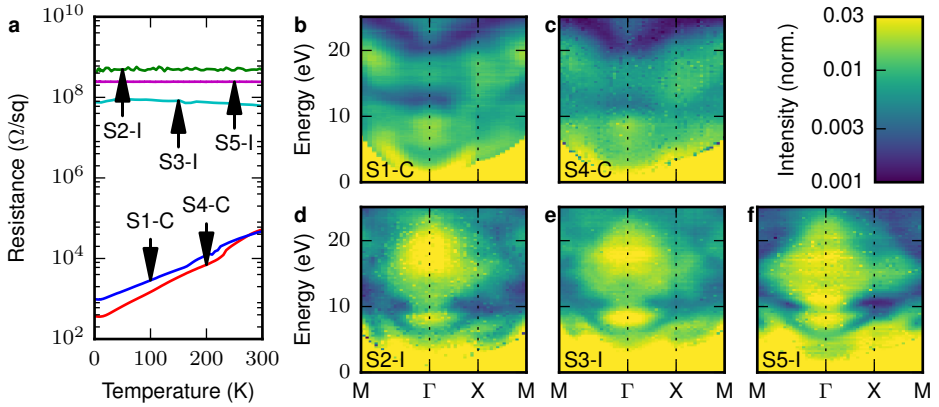

FIGURE 6.2: a) Sheet resistance versus temperature for five different samples. b-f) ARRES measurements for conducting (S1-C, S4-C) and non-conducting (S2-I, S3-I, S5-I) samples. Sample S1-C (b, blue) 8 u.c. $LaAlO_3$ grown in the LEEM, sample S4-C (c, red) 4 u.c. $LaAlO_3$ grown in a conventional PLD setup, sample S2-I (d, green) 8 u.c. $LaAlO_3$ grown with out-of-focus PLD laser, sample S3-I (e, cyan) 5 u.c. $LaAlO_3$ grown on SrO-terminated $SrTiO_3$ and sample S5-I (f, magenta) 5 nm $LaAlO_3$ grown with sputter deposition.

will elaborate on below. First we will characterize the electrical properties of these samples. For this, the temperature dependence of the sheet resistance is measured. The result is shown in fig. 6.2a for sample S1-C (blue), sample S2-I (green) and sample S3-I (cyan). Sample S1-C shows conducting behavior while sample S2-I and sample S3-I are insulating.

To fingerprint the difference between conducting and insulating samples at the growth temperature, we use angle-resolved reflected electron spectroscopy (ARRES)[14] as shown in fig. 6.2. ARRES utilizes the fact that the electron reflectivity strongly depends on the electron landing energy E_0 and the in-plane momentum $k_\parallel$. In particular the electron reflection is low if the material has a band at the specific (E_0, $k_\parallel$) of the electron so that it can couple into the band. In contrast, when (E_0, $k_\parallel$) of the electron coincide with a band gap the electron reflectivity is high. Hence the "reflected-electron" or ARRES map shows a fingerprint of the unoccupied band structure[(1)].

ARRES maps of sample S1-C, S2-I and S3-I are shown in fig. 6.2b, d and e respectively. These maps were measured directly after growth, at the growth temperature. The conducting sample S1-C (Fig. 6.2b) shows a band (minimum in intensity) around 14 eV at the Γ-point and a V-shaped band at the top of the figure above 20 eV, while the insulating samples S2-I and S3-I (Fig. 6.2d, and e) shows a maximum (i.e. a band gap) between 14 and 22 eV around the Γ-point. This clear and strong difference between a conducting and non-conducting samples raises the question if this correlation is general.

[(1)] Multiple scattering effects can influence the result.

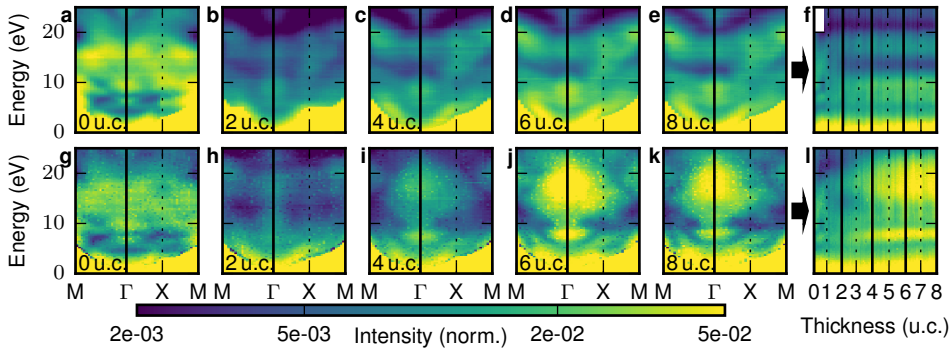

FIGURE 6.3: Conducting sample S1-C (top a-f) and non-conducting sample S2-I (bottom, g-l). From left to right ARRES maps for 0 (a, g), 2 (b, h), 4 (c, i), 6 (d, j) and 8 (e, k) unit cells respectively and an IV-curve versus thickness map (f, l). The black vertical lines at the Γ-point in the ARRES maps correspond with the black vertical lines in the IV-curve map including left and right edge. All images have the same color intensity.

For this we compare our samples with two more samples grown in other systems which are known from literature to produce conducting and non-conducting samples. These samples are sample S4-C grown in a conventional PLD system with the possibility to grow under higher oxygen pressures and known to result in conducting samples; and sample S5-I grown by on-axis sputter deposition, known to result in insulating samples[6]. ARRES maps are shown in figure 6.2c and f for the sample S4-C and S5-I respectively. Their (non-)conductance is confirmed by electrical measurements (Fig. 6.2a). During the ARRES measurements, both samples were kept at a high temperature in an oxygen pressure of 5×10^{-5} mbar to remove any contaminants and prevent the surface from charging. Exact growth and measurement conditions can be found in the appendix. Comparing S1-C and S4-C we conclude the ARRES map is stable under ex-situ transfer and against heating. The insulating samples S2-I, S3-I and S5-I in the bottom row of fig. 6.2 are similar, independent of how they are made. Remarkably, we find a clear difference between conducting and non-conducting samples at the growth temperature. Due to surface charging we cannot measure at room temperature, but the ex-situ grown and transferred samples S4-C and S5-I show our electron reflectivity measurements are stable.

Until now we focused on samples exceeding the critical thickness of four unit cells, required for samples to show conductivity[2]. Next we consider the influence of the thickness on the electron reflectivity, by measuring changes in the ARRES map during growth. Fig. 6.3 shows ARRES maps at the growth temperature for every second unit cell grown. Conducting sample S1-C is shown at the top (Fig. 6.3a-e) and insulating sample S2-I at the bottom (Fig. 6.3g-k). Both samples start with a TiO_2-terminated $SrTiO_3$ surface (a, g), showing the same ARRES map only slightly different in brightness. The ARRES maps show a strong change

as soon as two unit cells of $LaAlO_3$ are grown (b, h). However, the maps of the conducting sample S1-C (top, b) and insulating sample S2-I (bottom, h) still show many similarities. This changes at four unit cells of $LaAlO_3$. While for the conducting sample S1-C (Fig. 6.3c) the band around Γ at 14 eV becomes a little bit more pronounced compared to two unit cells, the non-conducting sample S2-I (Fig. 6.3i) strongly changes and develops a pronounced band gap around the Γ-point for energies between 14 and 22 eV, observed as a high-intensity area. Adding more $LaAlO_3$ up to 6 (Fig. 6.3d, j) and 8 (Fig. 6.3e, k) unit cells only leads to little changes, both for the conducting and the non-conducting samples.

To probe the changes during growth in more detail we focus on the electron reflectivity at the Γ-point ($k_{\|} = 0$). This is nothing else than a LEEM (or LEED) IV-curve, which is the intensity variation of a diffracted beam, in this case the specular beam, as function of electron energy. Such curves are indicated with a vertical black line in the ARRES maps in fig. 6.3. These curves were taken during growth at regular intervals of 8 to 10 times per unit-cell. Results are shown in fig. 6.3f and l (sample S1-C top (f) and sample S2-I bottom (l)). They show the gradual change from the $SrTiO_3$ fingerprint to the final IV-curve of the $SrTiO_3/LaAlO_3$ heterostructure. The five black vertical lines (including the edges) correspond to the vertical black lines at the Γ-point in the five ARRES maps on the left side of fig. 6.3.

The IV-curve map fig. 6.3f shows that the band at 14 eV in sample S1-C appears just after two unit cells have been grown. The band around 21 eV has already appeared at this thickness. The non-conducting sample S2-I (Fig. 6.3l) shows both bands around two unit cells, but they vanish between three and four unit cells when the band gap appears between 14 and 22 eV. The band gap at 8 eV also clearly appears at this thickness.

A zoomed-in part of the IV-curve maps in figure 6.3f and l, for zero to five unit cells, is shown in figure 6.4a and b together with an IV-curve map of sample S3-I with $LaAlO_3$ on SrO-terminated $SrTiO_3$ (Fig. 6.4c), the substrate prepared in a different PLD system. For comparison, the IV-curves after deposition of 0, 2 and 5 unit cells of $LaAlO_3$ are plotted in figure 6.4d, e and f. Here the IV-curves from sample S1-C (Fig. 6.4a) are plotted in blue, sample S2-I (Fig. 6.4b) in green and sample S3-I (Fig. 6.4c) in red. These plots show clearly two distinct starting (0 u.c.) IV-curves and two distinct IV-curves after deposition of 5 u.c. of $LaAlO_3$. The starting IV-curves correspond with the TiO_2- (blue, green) and SrO-terminated (red) $SrTiO_3$ while in the IV-curves after deposition we distinguish the conducting (blue) and non-conducting (green, red) samples.

The transition from the starting to the after-growth curve is different for the two insulating samples. This is very clear around two unit cells where sample S2-I (green) is still close to sample S1-C (blue) and not to sample S3-I (red), which is already close to the insulating final IV-fingerprint found on the non-conducting samples. As a matter of fact, the IV-curves for S3-I hardly change during growth on the SrO-terminated surface.

With these results, we can return to figure 6.1, where for sample S1-C (Fig 6.1b)

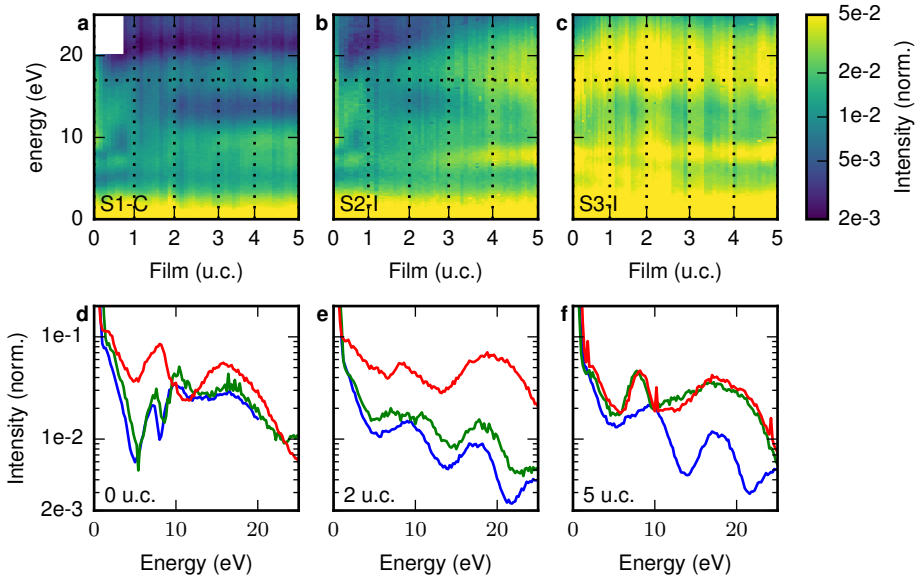

FIGURE 6.4: IV-curve versus thickness maps for sample S1-C (a), sample S2-I (b) and sample S3-I (c). d, e, f) IV-curves after deposition of 0, 2 and 5 unit cells of $LaAlO_3$, respectively, for sample S1-C (blue), sample S2-I (green) and sample S3-I (red). Horizontal dotted lines in a,b and c indicate the energy where fig. 6.1 is measured. IV-curves are obtained by the integrated intensity of the specular diffraction spot, filtering out any influence of the surface roughness.

the intensity strongly decreased at the start and continued to oscillate around a low value; for sample S2-I (Fig 6.1c) the intensity decreased at the start, but recovered between three and five unit cells; and for sample S3-I (Fig 6.1d) the intensity oscillated around the start value, and did not decrease at all. The energy of 17 eV where the data of fig. 6.1 was taken is indicated with a horizontal dotted line in the IV-curve maps, fig. 6.4a, b and c. Note that in fig. 6.1 the maximum of the specular diffraction spot is plotted, which is sensitive to spot broadening due to surface roughening. This results in growth oscillations superimposed on the electron reflectivity signal. On the other hand, for fig. 6.4 the intensity of the total specular spot is integrated, resulting in an intensity independent of spot shape (i.e. surface roughness) and only depending on the electron reflectivity. Combining fig. 6.1 and 6.4 we can now conclude that the increasing background signal between three and four unit cells in fig. 6.1c is caused by the appearance of the band gap shown in fig. 6.4b.

One question which may be raised with respect to the out-of-focus grown sample is whether the epitaxy is impaired by the ill-defined fluence. For that we performed a scanning transmission electron microscopy (STEM) experiment with high-angle annular dark-field imaging (HAADF) on sample S6-I, grown under the

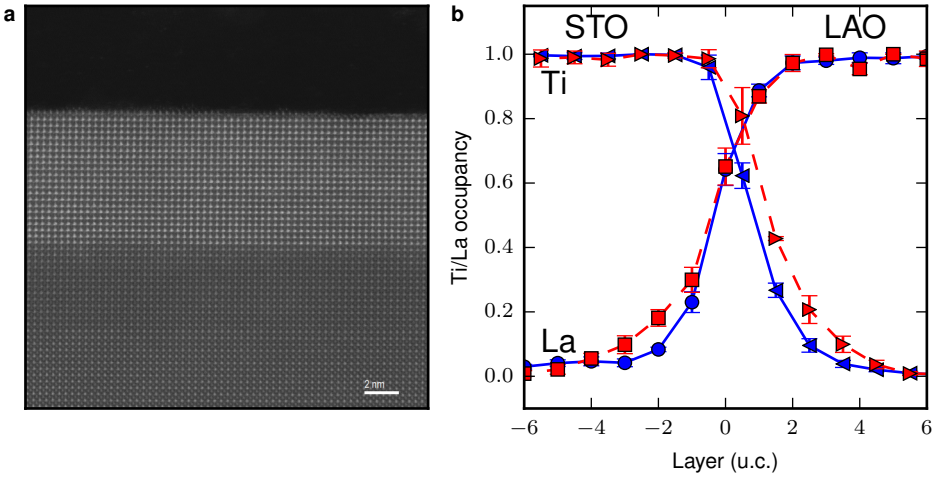

FIGURE 6.5: a) STEM-HAADF image of sample S6-I grown under same circumstances as S2-I, but with 20 unit cells of $LaAlO_3$. A slight misorientation between film and substrate can be observed. b) Normalized Ti- (◁, ▷) and La-occupancy (○, □) for S7-C, (blue, solid line, ○ and ◁) and S6-I (red, dashed line, □ and ▷). Sample S7-C has been grown under same conditions as S4-C. (experiment by N. Gauquelin, Antwerp)

same conditions as the out-of-focus sample S2-I, but with 20 unit cells $LaAlO_3$. The experiment also yields the concentration variation of the various elements when going through the interface. The results are shown in figure 6.5. Besides a slight misorientation, nice epitaxial growth can be observed. Figure 6.5b shows the Ti- and La-occupancy normalized to the total A- and B-site occupancy for the samples S6-I and S7-C. The sample S7-C is grown under comparable conditions as sample S4-C. Ti-diffusion into the $LaAlO_3$ can be observed for the out-of-focus sample S6-I, compared to the conducting sample S7-C.

6.4 Discussion

Even after many years of research, the outstanding question with respect to understanding the conductivity of the $SrTiO_3/LaAlO_3$ interface still is whether that is due to the electronic reconstruction of a basically perfect interface, or that defect generation in the $SrTiO_3$ is an essential ingredient. Secondary questions then exist about the role of intermixing, oxygen vacancies, the strain gradients and the ensuing buckling of the oxygen octahedra at the interface, or the stoichiometry of the $LaAlO_3$ layer. Central to the discussion are the two observations that conductance only occurs after growth on the TiO_2-terminated surface, not on the SrO-termination; and that 4 unit cells of $LaAlO_3$ are required to generate conductance. Especially the latter fact is often used to argue electronic reconstruction: the potential build-up in the polar $LaAlO_3$ is countered by charge transfer to the

interface after reaching a critical thickness. On the other hand, the importance of defects is supported by the observation of the influence of oxygen [7] and La/Al-stoichiometry [4–6] on the conductance.

The discussion on the La/Al-stoichiometry has started relatively recently. It has been found that the $LaAlO_3$ film has to be Al-rich for conductance to appear [4,5] and also that the $LaAlO_3$ stoichiometry is strongly dependent on the PLD parameters [22]. We will now argue that our electron reflectivity experiments precisely address the issue of (non-)stoichiometry and defects, which are crucial for the occurrence of interface conductivity. Our observations are that (i) the difference between C- and I-samples is already apparent during growth and at the growth temperature and (ii) the differences between C- and I-samples are significant on the scale of eVs. The conclusion we draw from this is that the (electronic) structure of the $LaAlO_3$ surface layer which is the one we are most sensitive to, is different for C-samples and for I-samples. The sensitivity of the electron reflectivity to the surface layer can be concluded from the strong change in IV-curve seen in figure 6.4d between TiO_2-terminated and SrO-terminated $SrTiO_3$. We note that the sensitivity depends on the penetration depth, which is energy dependent. Unfortunately, we cannot compare our data to calculations of the electron reflectivity, or the empty band structure of different possible surfaces. We can however sketch a scenario which can be contemplated for such calculations.

The scenario is as follows. We note that the $LaAlO_3$ grown on TiO_2-terminated $SrTiO_3$ should be AlO_2-terminated, while the $LaAlO_3$ grown on SrO-terminated $SrTiO_3$ should be LaO-terminated. We surmise that this difference in termination causes the strong difference between the conducting sample S1-C and the non-conducting sample S3-I. The most intriguing sample is S2-I, which shows an IV-curve comparable to sample S1-C (AlO_2-terminated) for two unit cells (Fig. 6.4e) and changes to the signature of sample S3-I (LaO-terminated) for five unit cells (Fig. 6.4f). In contrast to the other samples, sample S2-I was grown with an out-of-focus laser. As stated before, from literature we know that changing the PLD parameters, in particular the fluence, changes the stoichiometry of the grown film. Furthermore, we know that Al-rich $LaAlO_3$ results in a conducting interface and La-rich $LaAlO_3$ in an insulating interface. From this we infer sample S2-I with out-of-focus laser is La-rich. This together with the growth on TiO_2-terminated $SrTiO_3$ suggests the following. We start with the growth on TiO_2-terminated $SrTiO_3$ resulting in a AlO_2-termination, as seen after growth of two unit cells. Growing further the La-excess slowly builds up, changing the surface to LaO-rich. We further note that the Ti-intermixing into the $LaAlO_3$ found for sample S2-I could compensate the Al-deficits in the first unit cells, suppressing the effects of the La-excess in the first two unit cells.

Here we should remark that DFT calculations in Ref. 23 showed that the surface is not AlO_2- or LaO-terminated, but rather that $Al_{3/2}O_2$ and $La_{5/6}O$ are the stable surface terminations. This implies that the AlO_2 surfaces mentioned above are actually $Al_{3/2}O_2$ and the LaO surface are $La_{5/6}O$, which does not conflict with our results. On the contrary, the fact that less La is required for the $La_{5/6}O$ and

more Al for the $Al_{3/2}O_2$ surface could stimulate the transition from a $Al_{3/2}O_2$ to a $La_{5/6}O$ surface for our La-rich sample S2-I. In any case, the La-enrichment at the surface appears to be stronger than concluded in Ref. 23, which would certainly influence charge transfer to the interface.

Summarizing, we find that the strong change in electron reflectivity, which is correlated to the unoccupied band structure, depends on the surface termination. From the importance of the surface for the interface conductivity as described in literature[24,25] and our findings deduce that the excess La on the surface could be an essential step in suppressing the electron transfer to the interface. More research has to be done to investigate what exactly happens here.

Finally, we note that our La-rich and Al-rich surface signatures do not correspond with the IV-curves measured on bulk mixed ordered terminated $LaAlO_3$ measured in chapter 4. This can however be explained by the surface reconstructions found on the bulk $LaAlO_3$ and the difference between bulk and strained thin films.

6.5 Summary

We have shown results of electron reflectivity experiments (ARRES) on conducting and insulating $LaAlO_3/SrTiO_3$-heterostructures during growth, at the growth temperature with sub-unit cell precision. We find distinct signatures for the conducting and non-conducting samples independent of their growth conditions. In other words, the electron reflectivity (ARRES) can predict during growth whether a sample will be able to show conductivity.

We find that the two families of reflectivity curves (maps) can be assigned to the surface termination being either AlO_2 or LaO-rich. For samples with Al-rich $LaAlO_3$ the surface termination is directly couples to the termination of the $SrTiO_3$. A SrO-termination results in a LaO-rich surface, while a TiO_2-termination results in an AlO_2-rich surface. For the growth of La-rich $LaAlO_3$, which we believe we achieve by out-of-focus laser growth, we find the surface termination slowly changes from AlO_2-rich to LaO-rich during growth. From the importance of the surface for the interface conductivity as described in literature[24,25], we infer that it could be this change in surface termination that is essential in suppressing the interface conductivity for the La-rich growth.

6.6 Appendix

Five samples have been grown for LEEM analysis. The PLD and sputter growth parameters of this films are shown in table 6.1 together with the temperature where the ARRES maps are measured.

Sample Nr.	Fluence J/cm^2	Growth °C	Termination	Pressure mbar	Measure °C
S1-C	2	780	TiO_2	5×10^{-5}	795
S4-C	1	720	TiO_2	$1{\times}10^{-4}$	630
S2-I		770	TiO_2	5×10^{-5}	770
S3-I	2	700	SrO	5×10^{-5}	600
S5-I	na	830	TiO_2	$3{\times}10^{0}$	560

TABLE 6.1: PLD and sputter growth conditions for samples analyzed in LEEM as well as the temperature where the ARRES maps were taken.

References

[1] A. Ohtomo and H. Y. Hwang, *A high-mobility electron gas at the $LaAlO_3/SrTiO_3$ heterointerface*, Nature **427**, 423 (2004).

[2] S. Thiel, G. Hammerl, A. Schmehl, C. W. Schneider, and J. Mannhart, *Tunable Quasi-Two-Dimensional Electron Gases in Oxide Heterostructures*, Science **313**, 1942 (2006).

[3] L. Zhang, X.-F. Zhou, H.-T. Wang, J.-J. Xu, J. Li, E. G. Wang, and S.-H. Wei, *Origin of insulating behavior of the p-type $LaAlO_3/SrTiO_3$ interface: Polarization-induced asymmetric distribution of oxygen vacancies*, Physical Review B **82**, 125412 (2010).

[4] M. P. Warusawithana, C. Richter, J. A. Mundy, P. Roy, J. Ludwig, S. Paetel, T. Heeg, A. A. Pawlicki, L. F. Kourkoutis, M. Zheng, M. Lee, B. Mulcahy, W. Zander, Y. Zhu, J. Schubert, J. N. Eckstein, D. A. Muller, C. S. Hellberg, J. Mannhart, and D. G. Schlom, *$LaAlO_3$ stoichiometry is key to electron liquid formation at $LaAlO_3/SrTiO_3$ interfaces*, Nature Communications **4** (2013).

[5] E. Breckenfeld, N. Bronn, J. Karthik, A. R. Damodaran, S. Lee, N. Mason, and L. W. Martin, *Effect of Growth Induced (Non)Stoichiometry on Interfacial Conductance in* $LaAlO_3/SrTiO_3$, Physical Review Letters **110**, 196804 (2013).

[6] I. M. Dildar, D. B. Boltje, M. H. S. Hesselberth, J. Aarts, Q. Xu, H. W. Zandbergen, and S. Harkema, *Non-conducting interfaces of $LaAlO_3/SrTiO_3$ produced in sputter deposition: The role of stoichiometry*, Applied Physics Letters **102**, 121601 (2013).

[7] A. Brinkman, M. Huijben, M. van Zalk, J. Huijben, U. Zeitler, J. C. Maan, W. G. van der Wiel, G. Rijnders, D. H. A. Blank, and H. Hilgenkamp, *Magnetic effects at the interface between non-magnetic oxides*, Nature Materials **6**, 493 (2007).

[8] Ariando, X. Wang, G. Baskaran, Z. Q. Liu, J. Huijben, J. B. Yi, A. Annadi, A. R. Barman, A. Rusydi, S. Dhar, Y. P. Feng, J. Ding, H. Hilgenkamp, and T. Venkatesan, *Electronic phase separation at the $LaAlO_3/SrTiO_3$ interface*, Nature Communications **2**, 188 (2011).

[9] D. A. Dikin, M. Mehta, C. W. Bark, C. M. Folkman, C. B. Eom, and V. Chandrasekhar, *Coexistence of Superconductivity and Ferromagnetism in Two Dimensions*, Physical Review Letters **107**, 056802 (2011).

[10] J. A. Bert, B. Kalisky, C. Bell, M. Kim, Y. Hikita, H. Y. Hwang, and K. A. Moler, *Direct imaging of the coexistence of ferromagnetism and superconductivity at the $LaAlO_3/SrTiO_3$ interface*, Nature Physics **7**, 767 (2011).

[11] N. Reyren, S. Thiel, A. D. Caviglia, L. F. Kourkoutis, G. Hammerl, C. Richter, C. W. Schneider, T. Kopp, A.-S. Ruetschi, D. Jaccard, M. Gabay, D. A. Muller, J.-M. Triscone, and J. Mannhart, *Superconducting Interfaces Between Insulating Oxides*, Science **317**, 1196 (2007).

[12] A. Joshua, S. Pecker, J. Ruhman, E. Altman, and S. Ilani, *A universal critical density underlying the physics of electrons at the $LaAlO_3/SrTiO_3$ interface*, Nature Communications **3**, 1129 (2012).

[13] A. D. Caviglia, S. Gariglio, N. Reyren, D. Jaccard, T. Schneider, M. Gabay, S. Thiel, G. Hammerl, J. Mannhart, and J.-M. Triscone, *Electric field control of the $LaAlO_3/SrTiO_3$ interface ground state*, Nature **456**, 624 (2008).

[14] J. Jobst, J. Kautz, D. Geelen, R. M. Tromp, and S. J. van der Molen, *Nanoscale measurements of unoccupied band dispersion in few-layer graphene*, Nature Communications **6**, 8926 (2015).

[15] R. Tromp, J. Hannon, A. Ellis, W. Wan, A. Berghaus, and O. Schaff, *A new aberration-corrected, energy-filtered LEEM/PEEM instrument. I. Principles and design*, Ultramicroscopy **110**, 852 (2010).

[16] S. M. Schramm, J. Kautz, A. Berghaus, O. Schaff, R. M. Tromp, and S. J. van der Molen, *Low-energy electron microscopy and spectroscopy with ESCHER: Status and prospects*, IBM Journal of Research and Development **55**, 1:1 (2011).

[17] S. M. Schramm, A. B. Pang, M. S. Altman, and R. M. Tromp, *A Contrast Transfer Function approach for image calculations in standard and aberration-corrected LEEM and PEEM*, Ultramicroscopy **115**, 88 (2012).

[18] R. Tromp, J. Hannon, W. Wan, A. Berghaus, and O. Schaff, *A new aberration-corrected, energy-filtered LEEM/PEEM instrument II. Operation and results*, Ultramicroscopy (2013).

[19] M. B. S. Hesselberth, S. J. v. d. Molen, and J. Aarts, *The surface structure of $SrTiO_3$ at high temperatures under influence of oxygen*, Applied Physics Letters **104**, 051609 (2014).

[20] A. J. H. van der Torren, S. J. van der Molen, and J. Aarts, *Formation of a mixed ordered termination on the surface of* $LaAlO_3(001)$, Physical Review B **91**, 245426 (2015).

[21] M. Kawasaki, K. Takahashi, T. Maeda, R. Tsuchiya, M. Shinohara, O. Ishiyama, T. Yonezawa, M. Yoshimoto, and H. Koinuma, *Atomic Control of the $SrTiO_3$ Crystal Surface*, Science **266**, 1540 (1994).

[22] E. Breckenfeld, R. Wilson, J. Karthik, A. R. Damodaran, D. G. Cahill, and L. W. Martin, *Effect of Growth Induced (Non)Stoichiometry on the Structure, Dielectric Response, and Thermal Conductivity of $SrTiO_3$ Thin Films*, Chemistry of Materials **24**, 331 (2012).

[23] C. Weiland, G. E. Sterbinsky, A. K. Rumaiz, C. S. Hellberg, J. C. Woicik, S. Zhu, and D. G. Schlom, *Stoichiometry dependence of potential screening at $La_{(1-\delta)}Al_{(1+\delta)}O_3/SrTiO_3$ interfaces*, Physical Review B **91**, 165103 (2015).

[24] Y. Xie, C. Bell, T. Yajima, Y. Hikita, and H. Y. Hwang, *Charge Writing at the $LaAlO_3/SrTiO_3$ Surface*, Nano Letters **10**, 2588 (2010).

[25] R. Pentcheva, R. Arras, K. Otte, V. G. Ruiz, and W. E. Pickett, *Termination control of electronic phases in oxide thin films and interfaces: $LaAlO_3/SrTiO_3(001)$*, Philosophical Transactions of the Royal Society A: Mathematical, Physical and Engineering Sciences **370**, 4904 (2012).